J Mater Sci: Mater Electron (2017) 28:2877–2886
DOI 10.1007/s10854-016-5872-8

Magnetic and photo-catalyst Fe_3O_4–Ag nanocomposite: green preparation of silver and magnetite nanoparticles by garlic extract

Shahab Khaghani[1] · **Davood Ghanbari**[1]

Received: 26 August 2016 / Accepted: 11 October 2016 / Published online: 14 October 2016

Abstract At the first step Fe_3O_4 nanoparticles were synthesized via a green hydrothermal method in the presence of garlic (Allium sativum) extract. Then silver nanoparticles and Fe_3O_4–Ag (90 %:10 % and 50 %:50 %) nanocomposites were synthesized by hydrothermal method. The prepared products were characterized by X-ray diffraction pattern, scanning electron microscopy, and Fourier transform infrared spectroscopy. Vibrating Sample magnetometer illustrated that Fe_3O_4 nanoparticles have super-paramagnetic behaviour. The photo catalytic behaviour of Fe_3O_4–Ag nanocomposites was investigated using the degradation of four various azo dyes under ultraviolet light irradiation. The results show that nanocomposites have feasible magnetic and photo catalytic properties.

1 Introduction

Most technological and medical applications require monodisperse nanoparticles to have uniform physical and chemical properties. Small size and large surface-to-volume ratio leads to distinct magnetic properties which are different from those of their bulk structures [1]. This behaviour has been explained as due to the large volume fractions of the atoms in the grain boundary area with unusual properties like spin canting, surface anisotropy, dislocations and super-paramagnetic behaviour. Magnetic separation is considered as a high speed and effective technique for separating magnetic particles. Thus, if the powder adsorbent catalyst is magnetic, it could be recovered conveniently by magnetic field [1, 2]. Ferrites are technologically essential materials that are used in the fabrication of magnetic, electronic and microwave devices. These materials have a potential application at high frequency range due to their very low electrical conductivity, fairly large magneto-crystalline anisotropy, relatively large saturation magnetization, mechanical hardness low production costs [3, 4].

Hydrothermal synthesis can be defined as a method of synthesis of single crystals that depends on the solubility of minerals in hot water under high pressure. The crystal growth is performed in an apparatus consisting of a steel pressure vessel called an autoclave, in which a nutrient is supplied along with water. A temperature gradient is maintained between the opposite ends of the growth chamber. At the hotter end the nutrient solute dissolves, while at the cooler end it is deposited on a seed crystal, growing the desired crystal. Advantages of the hydrothermal method over other types of crystal growth include the ability to create crystalline phases which are not stable at the melting point. Also, materials which have a high vapour pressure near their melting points can also be grown by the hydrothermal method. The method is also particularly suitable for the growth of large good-quality crystals while maintaining control over their composition.

We have used hydrothermal method for this synthesis. Obviously hydrothermal is a unique method for fabricating nanostructures with specific and controlled morphologies. While predominant morphology.in other methods like sol–gel, sonochemical is nanoparticle. Hydrothermal method provides preferred orientation morphology. In hydrothermal method because of some particular conditions (high temperature and pressure) the nanoparticles grow in situ and form hierarchical structures [1, 4–6].

✉ Shahab Khaghani
Shahab.khaghani@gmail.com

[1] Young Researchers and Elite Club, Arak Branch, Islamic Azad University, Arak, Iran

There is a need to promote the experimental processes for the synthesis of nano-materials that offers ease in size control and stable preparation which could be used in wide range of applications. With the promotion of these new methods, the concern for environmental contamination is also heightened as chemical procedures generates a large amount of hazardous products. Hence, the focus has turned towards green chemistry and bioprocesses to establish clean, non-toxic, environmentally methods for nanoparticles production, such that the nanoparticles should be water-dispersible and stable in aqueous media for prolonged periods to be useful in biological applications. Micro-organisms, enzymes, plant biomass and plant extracts have shown a great potential as possible eco-friendly alternatives to chemical and physical methods. Using plant biomass/extract is more advantageous as compared to micro-organisms as it eliminates the elaborate time consuming processes of maintaining cultures [7]. Noble metals nanoparticles can strongly absorb visible light due to their localized surface plasmon resonance (LSPR), which can be adjusted by varying their size, surrounding and shape. When the frequency of the event light satisfies the resonance conditions of the noble-metal nanoparticles, the LSPR occurs with the associated light absorption. Moreover, noble metal nanoparticles can also work as an electron trap and active reaction sites [8–12]. Plasmon resonant nanostructures have gained remarkable interest in many fields, medicine, including near-field optics, surface enhanced spectroscopy, and solar cells. It was explored the applicability of plasmonic processes in the field of photocatalytic chemistry for organic molecule decomposition CO oxidation, and even materials synthesis. Various enhancement mechanisms have been proposed, comprising plasmonic heating and charge transfer [9, 10]. Noble metal nanoparticles have been the subject of extensive research in the frame of nanotechnology, mainly owing to their unique optical properties. Indeed, the free electron gas of such nanoparticles features a resonant oscillation upon illumination in the visible part of the spectrum. The spectral properties of this resonance depend on the constitutive material, the shape of the nanoparticles and its environment. This resonant electronic oscillation is called localized surface plasmon (LSP), and the field of research that studies the fundamentals and applications of LSP is known as nanoplasmonics. LSPs are accompanied

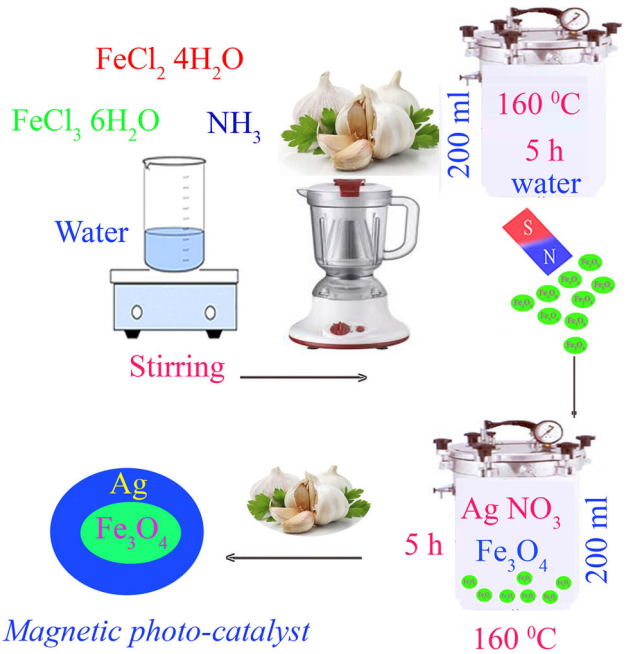

Fig. 1 Schematic of nanocomposite preparation

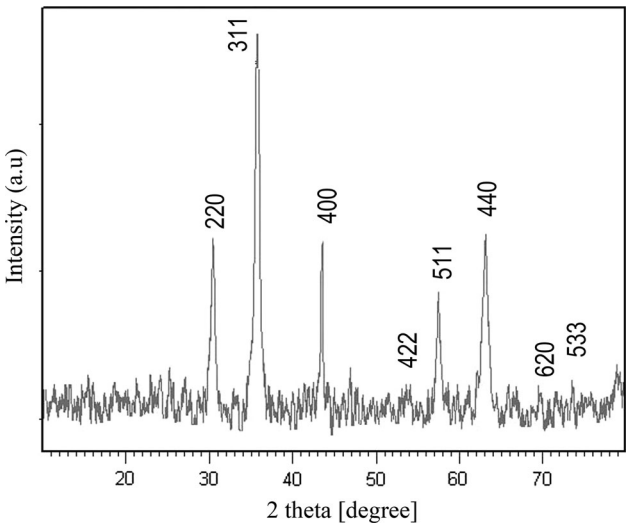

Fig. 2 XRD pattern of Fe_3O_4 nanoparticles

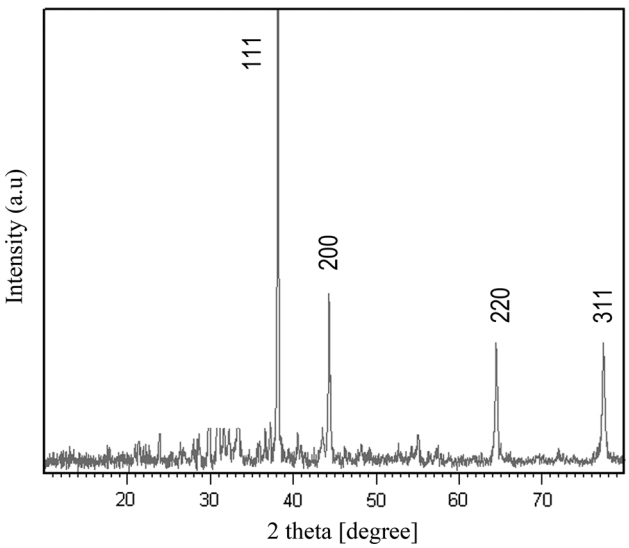

Fig. 3 XRD pattern of Ag nanoparticles

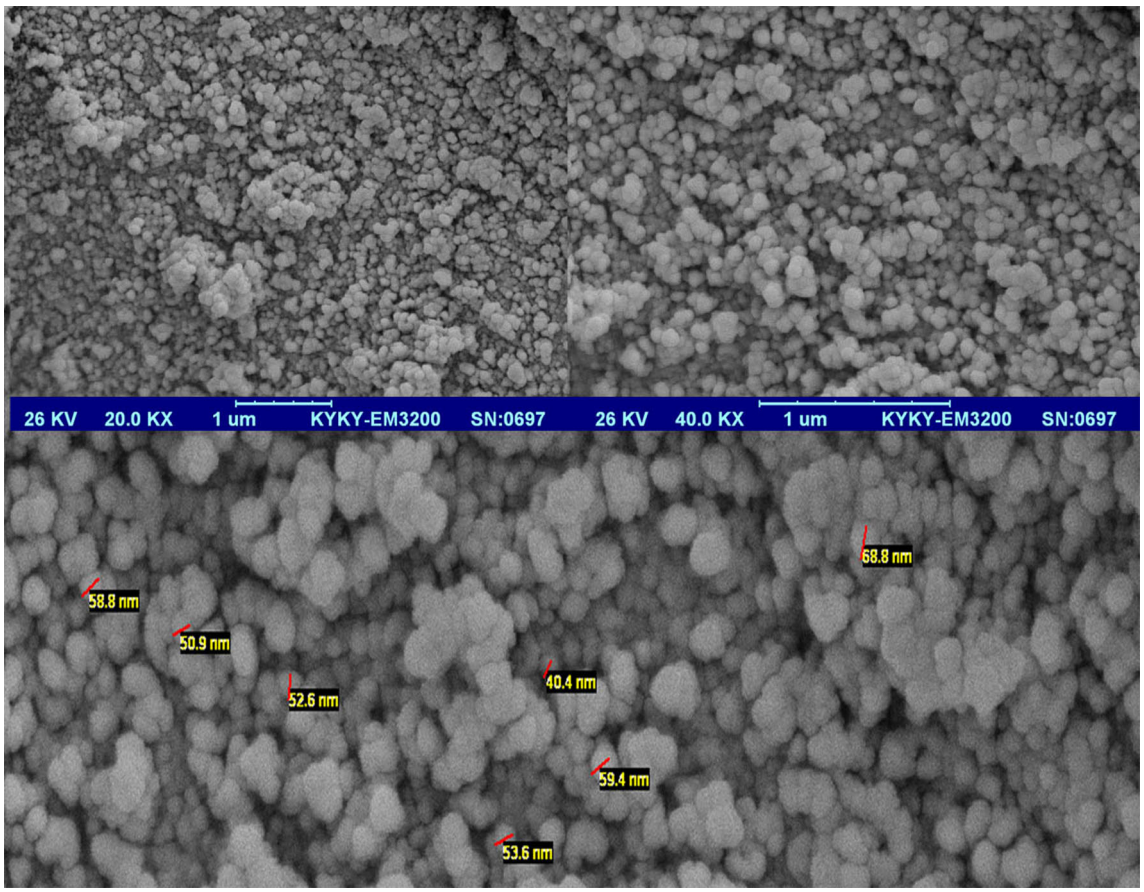

Fig. 4 SEM images of Fe_3O_4 by 2 ml of garlic extract at 160 °C

by valuable physical effects such as optical near-field enhancement, heat generation and excitation of hot-electrons. Hence, plasmonic nanoparticles can behave as efficient nanosources of heat, light or energetic electrons, remotely controllable by light [11, 12]. The composites of semiconductor nanoparticles and optically active metallic nanostructures represent a promising alternative to conventional photocatalysts. The main feature of these photocatalysts is that the interaction between semiconductor and metallic building blocks results in very efficient conversion of incident photons into electron–hole pairs in the semiconductor [12–15].

In this work Fe_3O_4–Ag nanocomposites were synthesized by green hydrothermal method with garlic juice. The photo catalytic behaviour of Fe_3O_4–Ag nanocomposites was evaluated using the degradation of three various azo dyes under ultraviolet light irradiation. The results show that nanocomposites have applicable super paramagnetic and photo catalytic performance.

2 Experimental

2.1 Materials and methods

$FeCl_3$ $6H_2O$, $FeCl_2$ $4H_2O$, $AgNO_3$, ammonia and distilled water were purchased from Merck Company and natural garlic (Allium sativum) juice was prepared. Scanning electron microscopy images were obtained using a LEO instrument model 1455VP. All the chemicals were used as received without further purifications. Before to taking images, the samples were coated by a very thin layer of Pt (using a BAL-TEC SCD 005 sputter coater) to make the sample surface conductor and prevent charge accumulation, and obtaining a better contrast. A multiwave ultrasonic generator (Bandeline MS 73), equipped with a converter/transducer and titanium oscillator, operating at 20 kHz with a maximum power output of 150 W was used for the ultrasonic irradiation. X-ray diffraction patterns were recorded by a Philips, X-ray diffractometer using Ni-

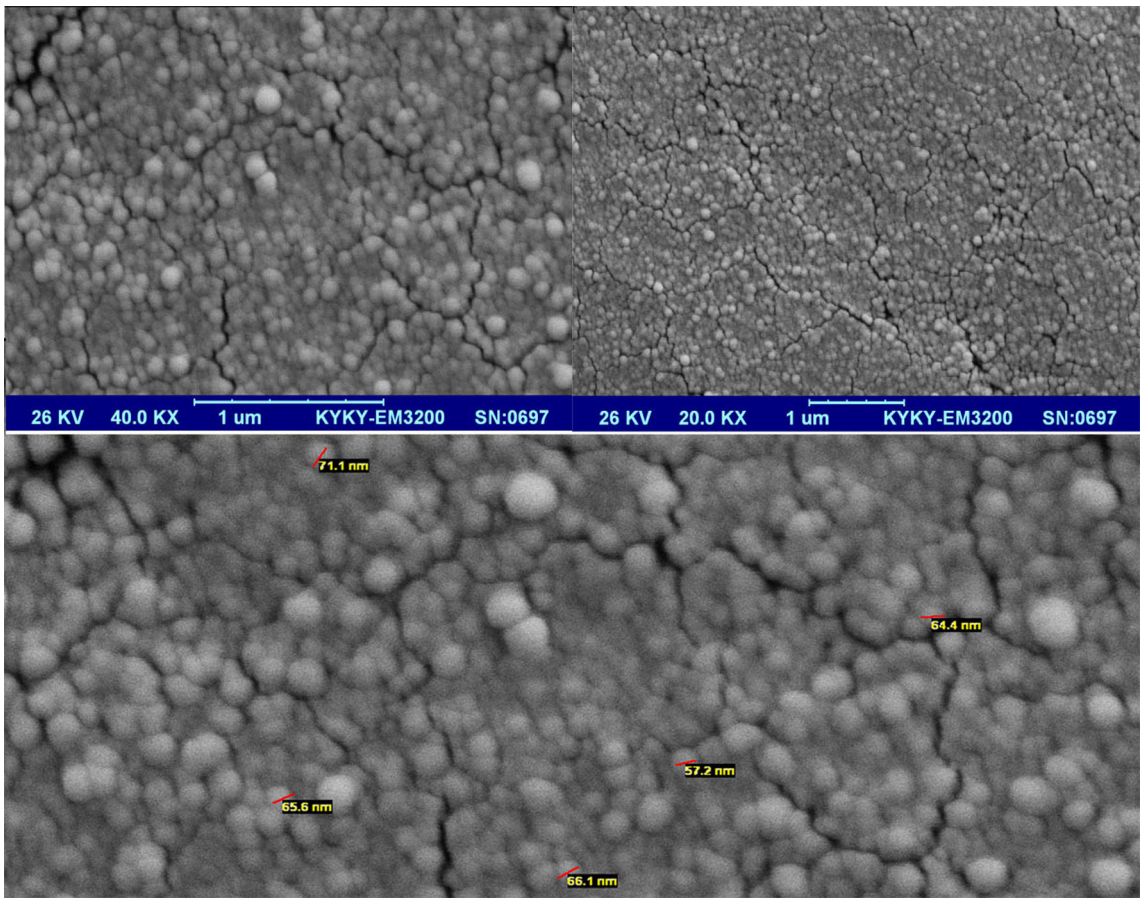

Fig. 5 SEM images of Fe_3O_4 by 10 ml of garlic extract at 160 °C

filtered CuKα radiation. Room temperature magnetic properties were investigated using a vibrating sample magnetometer (VSM) device, (Meghnatis Kavir Kashan Co., Iran) in an applied magnetic field sweeping between ±10,000 Oe.

2.2 Preparation of Fe_3O_4 nanoparticles

0.002 mol of $FeCl_3$ $6H_2O$ and 0.001 mol of $FeCl_2$ $4H_2O$ was dissolved in 200 mL of distilled water. Then 2–10 ml of garlic juice as surfactant was added to the solution, it was mixed on magnetic stirring for 10 min. 16 ml of NH_3 (1 M) as precipitator was slowly added to reaching pH of solution to 10. The solution is put into an autoclave and oven at 180 °C for 5 h. The obtained black precipitate was washed twice with distilled water. Then it was dried in oven for 24 h

2.3 Preparation of Fe_3O_4–Ag (50 %:50 %) and (90 %:10 %) nanocomposites

Firstly for preparation of Fe_3O_4–Ag (50 %:50 %), 0.1 g (50 %) of synthesized magnetite was dispersed in 200 ml of distilled water and then 0.2 g of $AgNO_3$ (Yield of Ag 0.1 g, 50 %) was then dissolved in the solution. Then 2 ml of garlic juice as surfactant was added to the solution and was mixed for 2 h. The solution is put into an autoclave and oven at 160 °C for 5 h, then it was calcinated at 400 °C for 2 h (Fig 1).

Also for preparation of Fe_3O_4–Ag (90 %:10 %) nanocomposite, 0.9 g (90 %) of magnetite was dispersed in

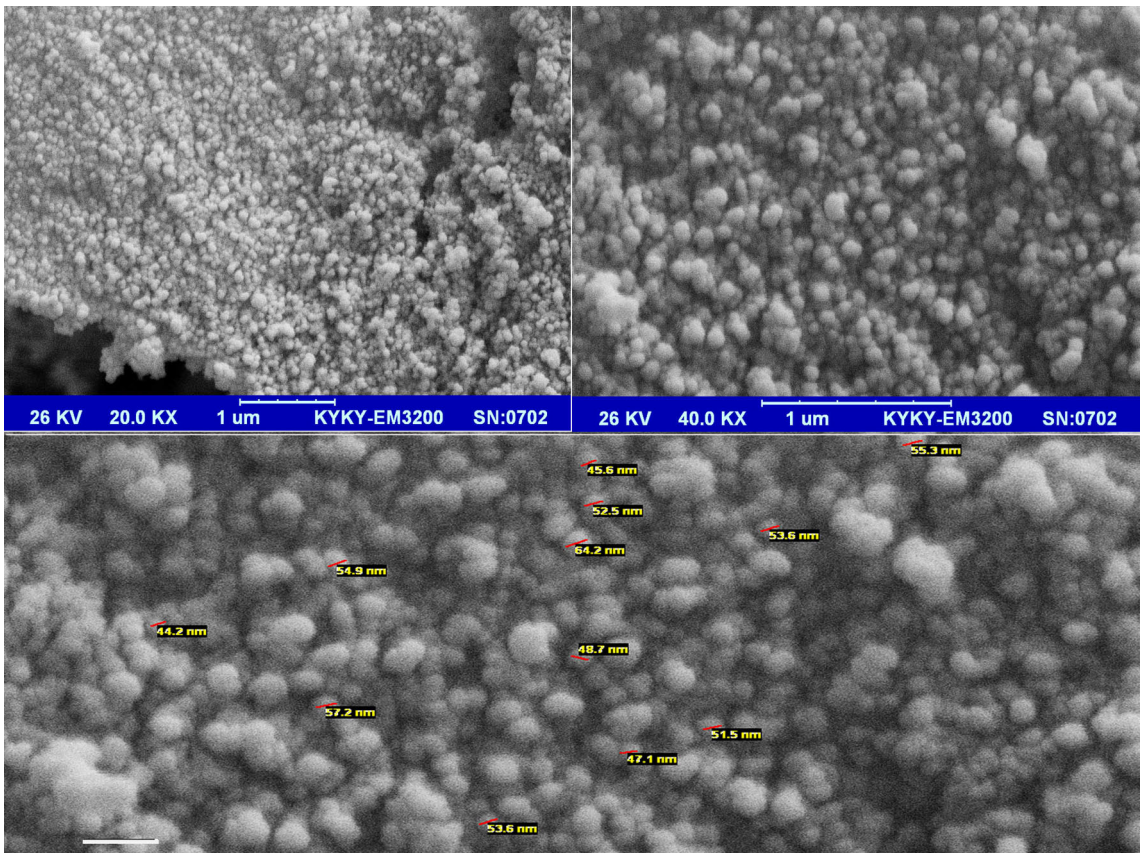

Fig. 6 SEM images of Fe_3O_4 by 2 ml of garlic extract at 200 °C

200 ml of distilled water and then 0.2 g of $AgNO_3$ (Yield of Ag 0.1 g, 10 %) was then dissolved in the solution.

2.4 Photo-catalyst investigation

10 ml of the dye solution (20 ppm) was used as a model pollutant to determine the photocatalytic activity. 0.1 g of catalyst was applied for degradation of 10 ml solution. The solution was mixed by a magnet stirrer for 1 h in darkness to determine the adsorption of the dye by catalyst and better availability of the surface. The solution was irradiated by a 10 W UV lamp which was placed in a quartz pipe in the middle of reactor. It was turned on after 1 h stirring the solution and sampling (about 10 ml) was done every 15 min. The samples were filtered, centrifuged and their concentration was determined by UV–visible spectrometry [13–15].

3 Results and discussion

Figure 2 illustrates XRD pattern of Fe_3O_4 product. It can be observed that cubic phase (JCPDS No.74-0748) with Fd-3 m space group which is consistent with pure magnetite was prepared. Figure 3 shows XRD pattern of silver product. A number of strong Bragg reflection peaks can be seen which correspond to the (111), (200), (220) and (311) reflections of FCC silver and lattice parameters of a = b, c = 4.070 Å. The standards (JCPDS), silver file No. 04-0783 and space group of Fm-3 m (space group number: 225) in the pattern are reported. The calculated crystalline sizes from Scherrer equation, $D_c = K\lambda/\beta Cos\theta$, where β is the width of the observed diffraction peak at its half maximum intensity (FWHM), K is the shape factor, which takes a value of about 0.9, and λ is the X-ray wavelength

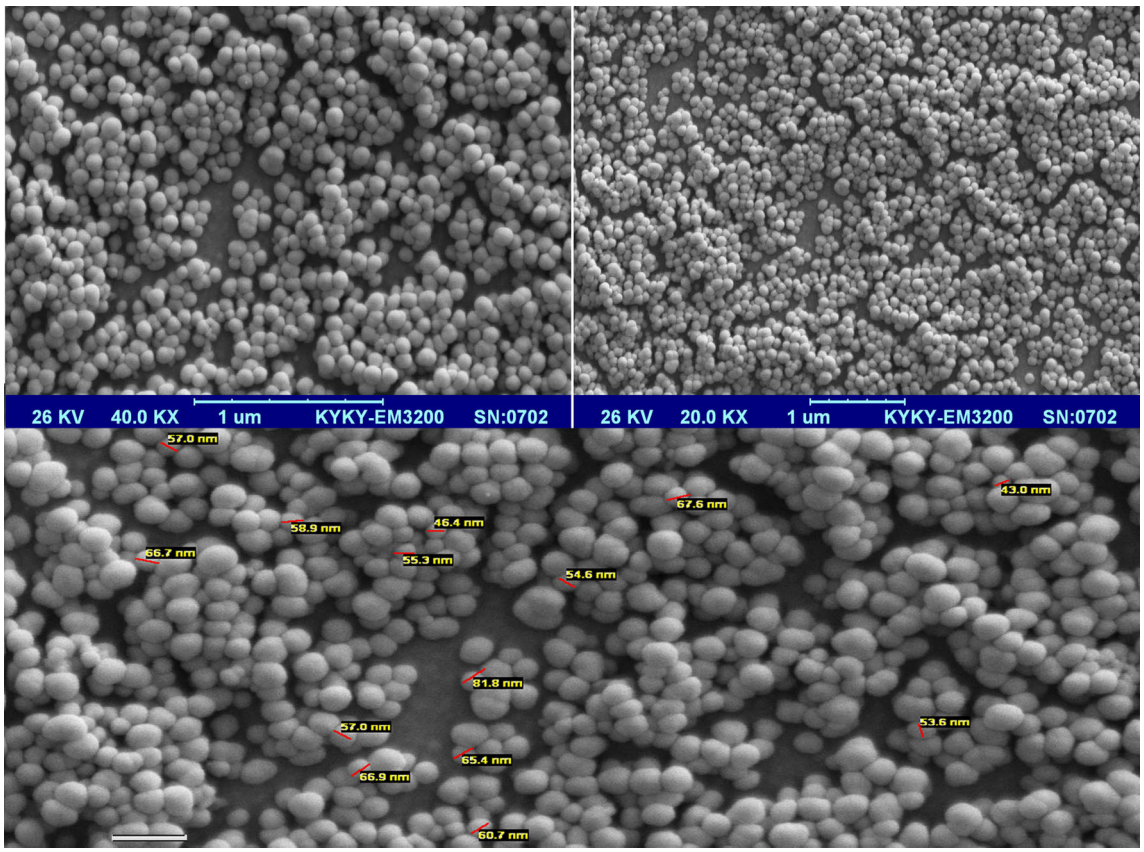

Fig. 7 SEM images of Ag by 2 ml of garlic extract at 160 °C

(CuK_α radiation, equals to 0.154 nm) were about 20 and 28 nm for Fe_3O_4 and Fe_3O_4–Ag nanoparticles, respectively.

SEM images of the as-synthesized Fe_3O_4 nanoparticles with 2 ml of garlic extract precursor at 160 °C are illustrated in Fig. 4. Nucleation stage overcomes to growth stage the and nanoparticles with average particle size less than 40 nm were synthesized.

Concentration effect of garlic extract was also examined. SEM images of the synthesized Fe_3O_4 nanoparticles with 10 ml of garlic juice as capping agent by hydrothermal method and heated in autoclave at 160 °C for 5 h are shown in Fig. 5. Results confirm by enhancement of garlic, size was increased and particles with average diameter size less than 90 nm were prepared.

The effect of temperature was also examined; Fig. 6 depict SEM images of the synthesized Fe_3O_4 nanoparticles with 2 ml of garlic juice as surfactant at 200 °C by hydrothermal method for 5 h. Images approve nanoparticles with average diameter size less than 50 nm were prepared.

SEM images of the synthesized Ag nanoparticles with 2 ml of garlic juice as surfactant by hydrothermal method and heated in autoclave at 160 °C in 5 h are shown in Fig. 7. Images confirm nanoparticles with average diameter size less than 20 nm were prepared.

The influence of higher amounts of garlic as tested, Fig. 8 illustrate SEM images of the synthesized Ag nanoparticles with 10 ml of garlic juice as surfactant at 160 °C. Results confirm agglomeration was observed and nanoparticles obtain with average diameter size less than 90 nm.

It is known that the particle size and morphology can be manipulated by adjusting the super-saturation during the

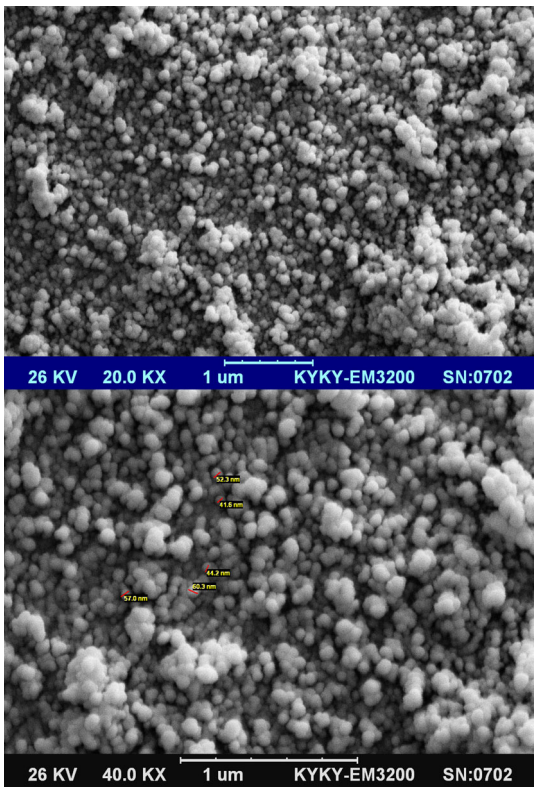

Fig. 8 SEM images of Ag by 10 ml of garlic extract at 160 °C

nucleation and crystal growth in hydrothermal, which in turn, it can strongly be affected by solution chemistry of hydrothermal conditions such as reaction temperature depends on precursor, time and temperature and pH of process environment.

Figure 9 show SEM images of Fe_3O_4–Ag (90 %:10 %) nanocomposites by 2 ml of garlic extract at 160 °C for 5 h. Images approve formation of nanostructures with average particle size around 50 nm. The balance between nucleation rate and growth rate which determines final particle size and morphology.

Figure 10 depicts the FT-IR spectrum of the as-prepared magnetite nanoparticles. The absorption peaks at 423 and 570 cm^{-1} are related to the Fe–O (metal–oxygen) stretching mode. The spectrum exhibits broad absorption peaks at 3310 cm^{-1}, assigned to the stretching mode of O–H group of adsorbed hydroxyl group and the weak band near 1640 cm^{-1} is corresponding to H–O–H bending vibration mode due to the adsorption of moisture on the surface of nanoparticles.

Magnetic properties of samples were studied using vibrating sample magnetometer system at room temperature. Hysteresis loop of magnetic Fe_3O_4 nanoparticles prepared by 2 ml of garlic extract at 160 °C is shown in Fig. 11. As-synthesized nanoparticles show super paramagnetic behaviour and have a saturation magnetization of 51 emu/g and a coercivity tending to zero Oe. It shows a sufficient magnetization of these nanoparticles for being recycled by a magnet, making them appropriate for core of recyclable photo-catalyst.

Hysteresis loop of magnetic Fe_3O_4–Ag 90–10 % nanoparticles prepared by simple hydrothermal is depicted in Fig. 12. The product also illustrates super paramagnetic behaviour and has a saturation magnetization of 40 emu/g and a coercivity about zero Oe.

Figure 13 shows hysteresis loop of magnetic Fe_3O_4–Ag 50–50 % nanoparticles prepared by hydrothermal at 180 °C. Nano-spheres show super paramagnetic behaviour and have a saturation magnetization of 21 emu/g and a coercivity about zero Oe. This magnetization indicates that Fe_3O_4–Ag nanocomposites inherit the magnetic property from the Fe_3O_4; however, the magnetization is lower due to presence of silver. This reduction in saturation magnetization is due to the interfacial effect of the typical nanocomposite. The magnetic property of the prepared nanocomposites is an essential characteristic of a re-generable and reusable magnetic heterogeneous catalyst.

The photo-catalytic activity of the Fe_3O_4–Ag (90–10 %) nanocomposite was evaluated by monitoring the degradation of Acid-Brown, Acid Blue, Acid Black and Acid Violet in an aqueous solution, under irradiation with UV light. The photo-degradation mechanism of silver under UV–visible absorption is illustrated in Fig. 14. The changes in the intensity of maximum wave length of four azo-dyes are depicted in Fig. 15. Maximum wave length of Acid-Brown, Acid Black, Acid Blue and Acid Violet were degraded about 98, 97, 80 and 75 % in 60 min in the presence of magnetite-silver. Acid brown showed the fastest degradation at 40 min under ultraviolet light and at presence of magnetic photo-catalyst. Organic dyes decompose to carbon dioxide, water and other less toxic or nontoxic residuals [14–18]. Figure 16 shows degradation

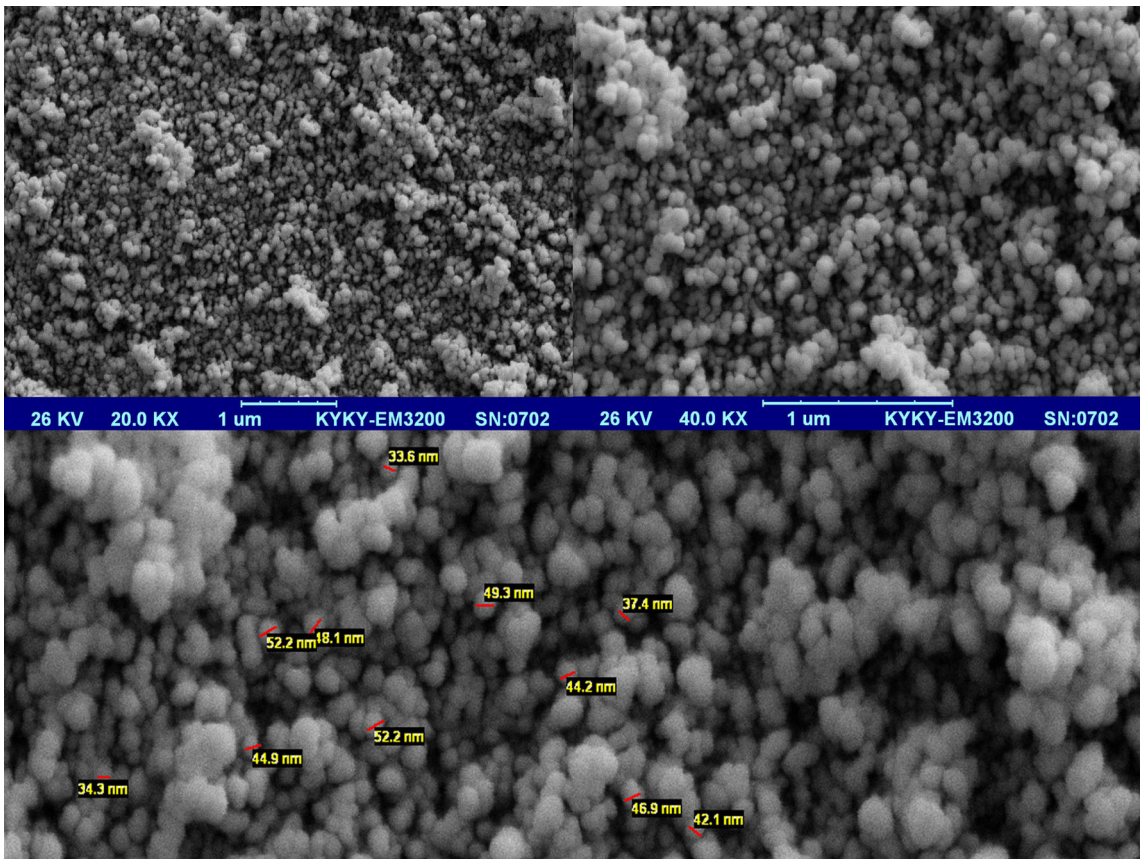

Fig. 9 SEM images of Fe_3O_4–Ag prepared (90 %:10 %) by 2 ml of garlic extract at 160 °C

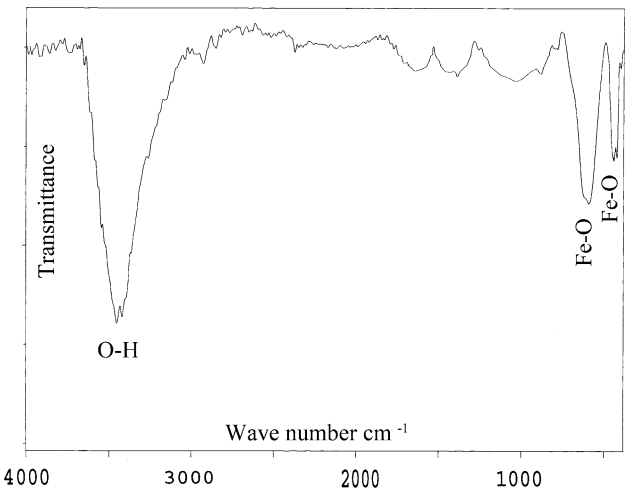

Fig. 10 FT-IR spectrum of Fe_3O_4 nanoparticles

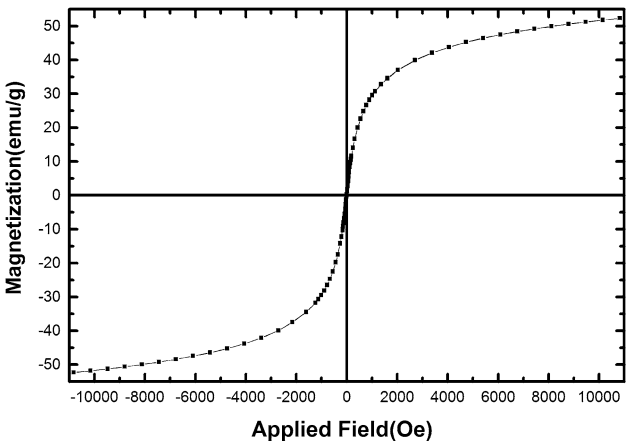

Fig. 11 Room temperature hysteresis loop of Fe_3O_4 nanoparticles

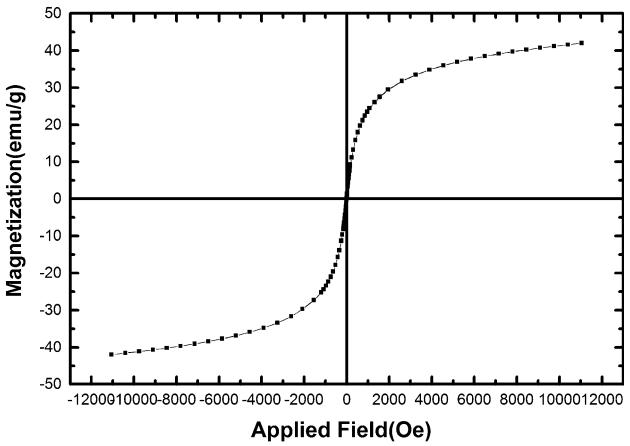

Fig. 12 VSM curve of Fe_3O_4–Ag 90–10 % nanocomposites

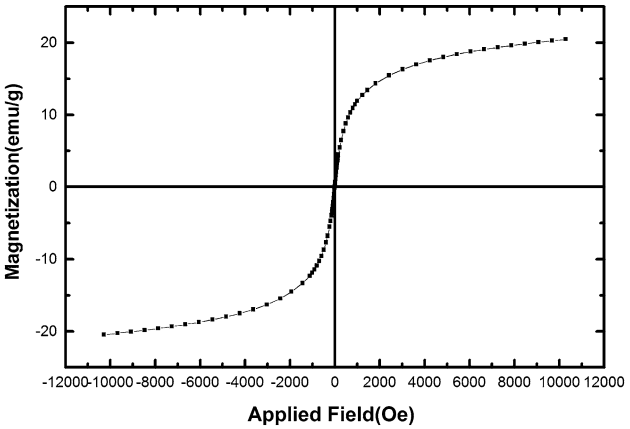

Fig. 13 Hysteresis curve of Fe_3O_4–Ag 50 %:50 % nanocomposite

of the three azo dyes after 60 min exposure to the Fe_3O_4–Ag nanocomposite.

4 Conclusions

Firstly magnetite nanoparticles were synthesized via a green hydrothermal in the presence of garlic juice, then silver nanoparticles and Fe_3O_4–Ag nanocomposites were prepared by hydrothermal method. Effect of temperature, reaction time and various concentration of garlic juice were investigated on the morphology and particle size of the products. Vibrating sample magnetometer confirmed that nanocomposites exhibit super-paramagnetic behaviour.

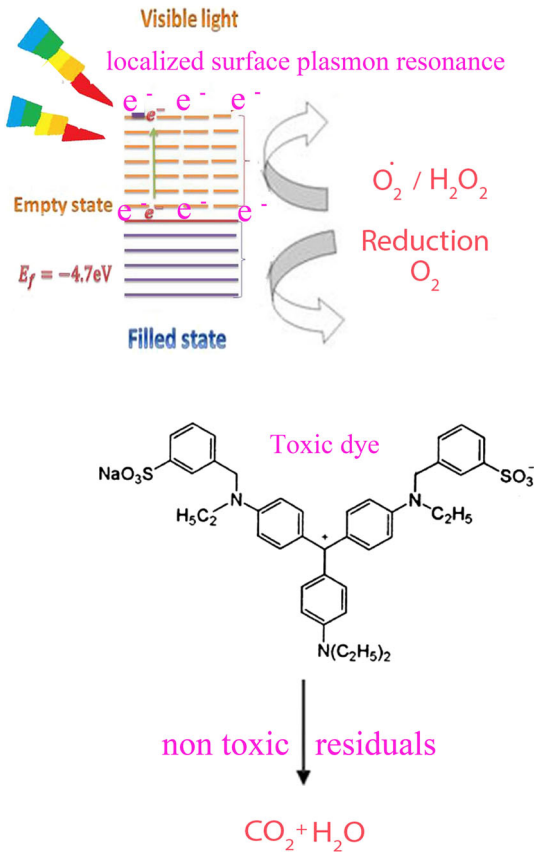

Fig. 14 Photo-catalyst mechanism of silver in degradation of toxic dye

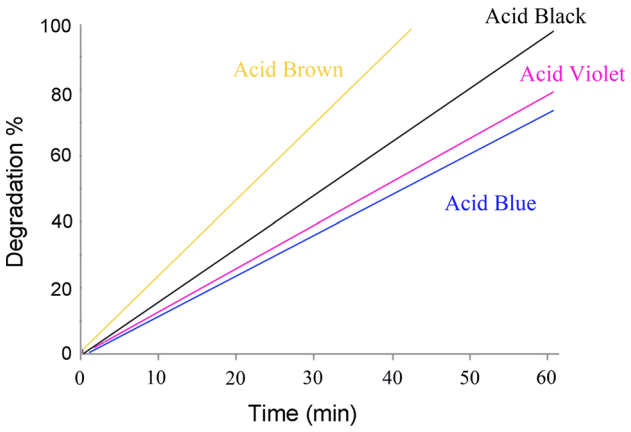

Fig. 15 Photo degradation of **a** acid brown **b** acid black **c** acid blue **d** acid violet (Color figure online)

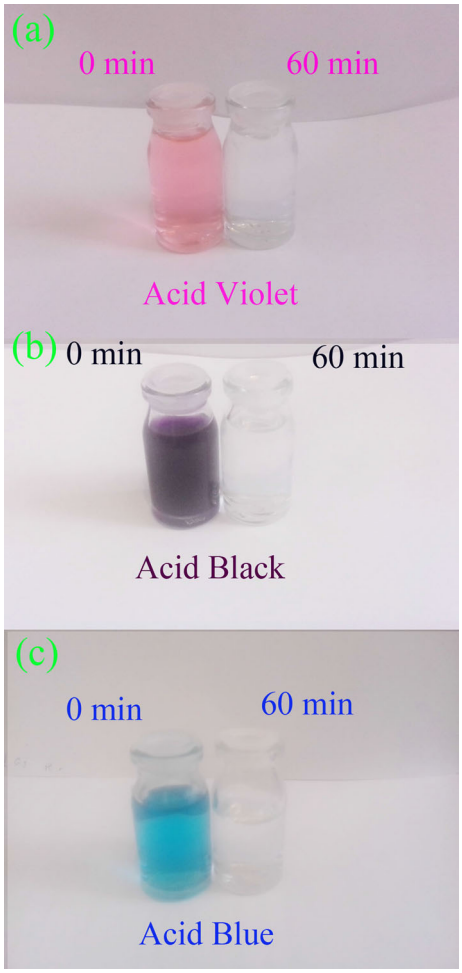

Fig. 16 Photo degradation of **a** acid violet **b** acid black **c** acid blue (Color figure online)

The photocatalytic behaviour of Fe_3O_4–Ag nanocomposite was evaluated using the degradation of three azo dyes under UV–visible light irradiation. The results show that hydrothermal method is suitable method for preparation of Fe_3O_4–Ag nanocomposites as a candidate for photocatalytic applications.

References

1. N. Asiabani, G. Nabiyouni, S. Khaghani, D. Ghanbari, J. Mater. Sci. Mater. Electron. (2013). doi:10.1007/s10854-016-5635-6
2. E. Manova, T. Tsoncheva, C.L. Estournes, D. Paneva, K. Tenchev, I. Mitov, L. Petrov, Appl. Catal. A **2**, 300 (2006)
3. D. Ghanbari, S. Sharifi, A. Naraghi, G. Nabiyouni, J. Mater. Sci.: Mater. Electron. **27**, 5315 (2016)
4. L. Rastogi, J. Arunachalam, Mater. Chem. Phys. **129**(1–2), 558–563 (2011)
5. R. Amooaghaie, M.R. Saeri, M. Azizi, Ecotoxicol. Environ. Saf. **120**, 400–408 (2015)
6. L. Rastogi, J. Arunachalam, Adv. Mat. Lett. **4**(7), 548–555 (2013)
7. S. Masoumi, G. Nabiyouni, D. Ghanbari, J. Mater. Sci. Mater. Electron. **27**, 9962 (2016)
8. P. Wang, B. Huang, Y. Daia, M.-H. Whangbo, Chem. Phys. **14**, 9813–9825 (2012)
9. W.J. Tseng, S.-M. KaoA, J.H. Hsieh, J. Ceram Int **04**, 139 (2015)
10. Z. Liu, W. Hou, P. Pavaskar, M. Aykol, S.B. Cronin, J. Nano Lett. **11**, 1111–1116 (2011)
11. G. Baffoua, R. Quidant, Chem. Soc. Rev. **43**, 3898–3907 (2014)
12. P. Christopher, D.B. Ingram, S. Linic, J. Phys. Chem. C **114**, 9173–9177 (2010)
13. A. Rezaei, G. Nabiyouni, D. Ghanbari, J. Mater. Sci. Mater. Electron. (2016). doi:10.1007/s10854-016-5258-y
14. A. Shabani, G. Nabiyouni, J. Saffari, D. Ghanbari, J. Mater. Sci. Mater. Electron. **27**, 8661 (2016)
15. J. Saffari, N. Mir, D. Ghanbari, K. Khandan-Barani, A. Hassan-abadi, M.R. Hosseini-Tabatabaei, J. Mater. Sci. Mater. Electron. **26**, 9591 (2015)
16. S. Masoumi, G. Nabiyouni, D. Ghanbari, J. Mater. Sci. Mater. Electron. **27**, 11017 (2016)
17. G. Nabiyouni, A. Ahmadi, D. Ghanbari, H. Halakouie, J. Mater. Sci. Mater. Electron. **27**, 4297 (2016)
18. F. Sadeghpour, G. Nabiyouni, D. Ghanbari, J. Mater. Sci. Mater. Electron. (2016). doi:10.1007/s10854-016-5370-z